

**Intrinsic surface superconducting instability in type-I Weyl semimetals**Aymen Nomani<sup>1</sup> and Pavan Hosur<sup>1,2</sup><sup>1</sup>*Department of Physics, University of Houston, Houston, Texas 77204, USA*<sup>2</sup>*Texas Center for Superconductivity, University of Houston, Houston, Texas 77204, USA* (Received 27 April 2023; revised 29 August 2023; accepted 18 September 2023; published 23 October 2023)

Recent experiments on nonmagnetic Weyl semimetals have seen separate bulk and surface superconductivity in Weyl semimetals, which raises the question of whether the surface Fermi arcs can support intrinsic superconductivity while the bulk stays in the normal state. A theoretical answer to this question is hindered by the absence of a well-defined surface Hamiltonian since the Fermi arcs merge with the bulk states at their endpoints. Using an alternate, Green's functions-based approach on a phenomenological model that can yield arbitrary Fermi arcs, we show—within mean-field theory—that the surface can support a standard Cooper instability while the bulk remains in the normal state. Although the surface has lower dimensionality, a higher density of states compared to the bulk allows it to have a higher mean-field superconducting transition temperature. The surface superconductivity is presumably of the Berezinskii-Kosterlitz-Thouless type.

DOI: [10.1103/PhysRevB.108.165144](https://doi.org/10.1103/PhysRevB.108.165144)**I. INTRODUCTION**

Weyl semimetals are three-dimensional (3D) topological materials defined by the presence of nondegenerate bands that intersect at discrete points in bulk momentum space [1–18]. These points are known as Weyl nodes because the low energy dispersion around them resembles that of a Weyl fermion. Weyl nodes have a well-defined chirality or handedness and occur in even numbers in a Weyl semimetal, with half of each chirality. They also carry topological protection in the sense they cannot be gapped out perturbatively while translational symmetry of the material persists; when it does not, they can only be annihilated in pairs of opposite chirality [19–39].

Many experiments have seen superconductivity in Weyl [40–57] and closely related Dirac semimetals [58–68] but recent experiments have hinted at independent intrinsic superconducting behaviours in the bulk and on the surface. In type-I Weyl semimetal t-PtBi<sub>2</sub>, transport measurements on bulk single crystals and thin films showed superconductivity with a  $T_C$  of 0.6 K [56] and 0.275–0.4 K, respectively [69]. The latter saw Berezinskii-Kosterlitz-Thouless behavior in surprisingly thick films, suggesting that the superconductivity may be of 2D origin. Scanning tunneling spectroscopy on the surface revealed a wide range of superconducting gaps with the largest gaps corresponding to  $T_C$  in the 100 K range [57]. Additionally, ARPES studies in t-PtBi<sub>2</sub> found a surface  $T_C$  of around 10 K where the bulk remained in normal state [70]. Powdered NbP was also found to exhibit superconductivity [46,47] with a small superconducting volume fraction, and Ref. [47] speculated that the superconductivity could be occurring on the surface. These observations raise the question, “Can the surface turn superconducting while the bulk remains in the normal state?”

The answer is hindered by another fundamental and exotic property of Weyl semimetals, namely surface states known as the Fermi arc. These are open strings of zero energy states on the surface of a Weyl semimetal that connect the surface

projections of Weyl nodes of opposite chirality. Unlike the Fermi surfaces of a conventional 2D metal, they do not form a closed contour; unlike the surface states of topological insulators, their penetration depth into the bulk depends strongly on the surface momentum and diverges at the end points, causing their wave function to merge with the bulk Bloch waves at the Weyl nodes [8–16,71–89]. The inseparability of the bulk and the surface makes it impossible to define a surface Hamiltonian, which hinders theoretical inquiries into the surface physics of Weyl semimetals. Nonetheless, the question raised above can be rephrased as “Does the Fermi arc metal support an intrinsic Cooper instability independently of the bulk?”

In this work, we explore the superconducting instability of the surface of time-reversal symmetric Weyl semimetals (TWSMs), since time-reversal symmetric Fermi surfaces generically have a superconducting instability, and discover an affirmative answer to the above question. Such an answer directly contrasts naïve expectations from Bardeen-Cooper-Schrieffer theory [90]. According to the theory, higher dimensionality suppresses fluctuations and stabilizes mean-field superconductivity, suggesting that the bulk of a TWSM should be more susceptible to superconductivity than the surface. However, we find that the surface can turn superconducting before the bulk does. This is because the surface has a finite density of states due to the Fermi arcs, whereas the bulk density of states vanishes in the Weyl limit and remains parametrically small for a slightly doped Weyl node.

In Sec. II, we introduce the general Hamiltonian for the Weyl semimetal and show how Green's function formalism bypasses the problem of surface-bulk inseparability. The interaction is introduced, which is an intralayer Hubbard interaction with pair hopping. This interaction is then used to calculate the correlation function that induces a surface superconducting instability. The problem then reduces to calculating the second-order bubble diagram. In Sec. III, we introduce a model of a TWSM with an arbitrary number and shape of Fermi arcs and the associated Green's function.

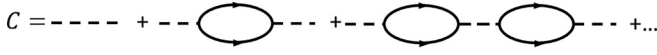


FIG. 1. The Dyson series for  $C_{\mathbf{K},iv_n}$  in the large- $D_S$  limit. Superconductivity occurs when  $C_{0,0}$  diverges.

Using this model, the contribution to the correlation function splits into two parts: the Fermi arcs and the projection of the bulk Fermi surface on the surface. The contribution due to Fermi arcs is then calculated in Sec. IV A, and in Sec. IV B we show the contribution due to the projection of the bulk states onto the surface. In Sec. V, we calculate the bulk instability. Finally, in Sec. VI, we discuss the implications of our result in the context of the experiments performed on NbP and t-PtBi<sub>2</sub>.

## II. GENERAL FORMALISM

In this section, we develop the formalism for studying the surface superconducting instability in a type-I Weyl semimetal. While a surface Hamiltonian is ill defined, a surface Green's function is meaningful and is the building block of our theory. Such an approach has previously been successful in evading this problem of bulk-surface inseparability and studying surface physics such as Friedel oscillations [75], conductivity [91], and Luttinger arcs [92].

We begin by considering a slab of a time-reversal symmetric Weyl semimetal described by the Bloch Hamiltonian  $H_{\mathbf{k}}$ . We assume  $2D_z$  degrees of freedom in the  $z$ th layer—the evenness mandated by time-reversal symmetry—and decompose  $H_{\mathbf{k}}$  into blocks capturing the surface, the bulk, and the surface bulk coupling:

$$H_{\mathbf{k}} = \begin{pmatrix} H_{\mathbf{k}}^S & h_{\mathbf{k}} \\ h_{\mathbf{k}}^\dagger & H_{\mathbf{k}}^B \end{pmatrix}. \quad (1)$$

Here,  $H_{\mathbf{k}}^S$  is the  $2D_S \times 2D_S$  in-plane Bloch Hamiltonian of the  $z = 0$  surface layer,  $H_{\mathbf{k}}^B$  is the Bloch Hamiltonian of all the other layers that we collectively refer to as “bulk,” while  $h_{\mathbf{k}}^\dagger$ ,  $h_{\mathbf{k}}$  capture the coupling between the bulk and the surface. The coupling terms can be strong, making it difficult to write an effective surface Hamiltonian, but an effective surface Green's function can be written. Specifically, writing Matsubara Green's function for the full slab in block form and evaluating the  $2D_S$ -dimensional block corresponding to the surface degrees of freedom yields an effective surface Green's function [92]

$$g_{\mathbf{k},i\omega_n} = (i\omega_n - H_{\mathbf{k}}^S - h_{\mathbf{k}} G_{\mathbf{k},i\omega_n}^B h_{\mathbf{k}}^\dagger)^{-1}, \quad (2)$$

where  $G_{\mathbf{k},i\omega_n}^B = (i\omega_n - H_{\mathbf{k}}^B)^{-1}$ .  $g_{\mathbf{k},i\omega_n}$  can alternately be obtained by integrating out the bulk fermions from a Euclidean path integral, see Appendix A. Importantly,  $g_{\mathbf{k},i\omega_n}$  can be calculated analytically for certain local hopping models, as we demonstrate shortly.

Next, in anticipation of deriving a large- $D_S$  mean-field theory, we introduce local, intralayer attractive Hubbard and pair-hopping interactions that are invariant under  $O(D_z)$  rotations within each layer. Explicitly,

$$H_{\text{int}} = - \sum_{\mathbf{r},z} \sum_{n_z,n'_z} \frac{U}{D_z} c_{\uparrow,\mathbf{r},z,n_z}^\dagger c_{\downarrow,\mathbf{r},z,n_z}^\dagger c_{\downarrow,\mathbf{r},z,n'_z} c_{\uparrow,\mathbf{r},z,n'_z}, \quad (3)$$

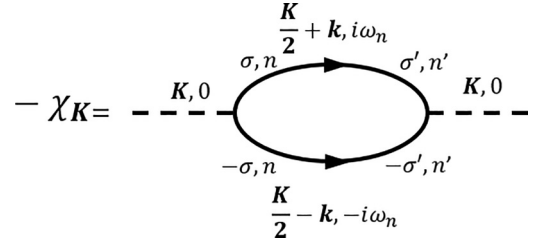


FIG. 2. The second order bubble diagram  $-\chi_{\mathbf{K}}$  helps us calculate  $C_{\mathbf{K},0}$ . Dashed (solid) lines denote bosons (fermions). The two fermion lines give two Green's functions that need to be summed over the internal momentum and frequency.

where  $U > 0$ ,  $n$  indicates the orbital index, and  $\mathbf{r}$  is the 2D position vector. Fourier transforming in-plane,

$$H_{\text{int}} = - \int_{\mathbf{k}',\mathbf{k},\mathbf{K}} \sum_{n_z,n'_z} \sum_z \frac{UV_{\text{cell}}}{D_z} c_{\uparrow,\frac{\mathbf{K}}{2}+\mathbf{k},z,n_z}^\dagger c_{\downarrow,\frac{\mathbf{K}}{2}-\mathbf{k},z,n_z}^\dagger \times c_{\downarrow,\frac{\mathbf{K}}{2}-\mathbf{k}',z,n'_z} c_{\uparrow,\frac{\mathbf{K}}{2}+\mathbf{k}',z,n'_z}, \quad (4)$$

where  $\mathbf{K}$ ,  $\mathbf{k}$ , and  $\mathbf{k}'$  are 2D momenta and  $\int_{\mathbf{k}} \equiv \int \frac{d^2k}{(2\pi)^2} \cdot V_{\text{cell}}$  is the volume of the unit cell, which will be set to one going forward for brevity.

We decouple  $H_{\text{int}}$  on the surface in the superconducting channel by introducing complex bosonic fields  $\Delta_{\mathbf{K},iv_n}$ ; see Appendix B for details. The superconducting instability then corresponds to the divergence of the correlation function  $C_{\mathbf{K},iv_n} = \langle \overline{\Delta_{\mathbf{K},iv_n} \Delta_{\mathbf{K},iv_n}} \rangle$  at  $\mathbf{K} = 0$ ,  $iv_n = 0$ . Long wave length equilibrium fluctuations about the mean-field state are subsequently captured by  $C_{\mathbf{K},0}$ . In the large  $D_S$  limit,  $C_{\mathbf{K},iv_n}$  is dominated by RPA-like bubble diagrams, which enables a straightforward resummation of the Dyson series, Fig. 1. The upshot is

$$C_{\mathbf{K},0} = - \frac{U/D_S}{1 - \frac{U}{D_S} \chi_{\mathbf{K}}}, \quad (5)$$

where  $-\chi_{\mathbf{K}}$  is the bubble shown in Fig. 2 and is given by

$$\chi_{\mathbf{K}} = \frac{1}{\beta} \sum_{i\omega_n} \int_{\mathbf{k}} \text{Tr}[g_{\mathbf{k}+\frac{\mathbf{K}}{2},i\omega_n}^T g_{\mathbf{k}-\frac{\mathbf{K}}{2},-i\omega_n}] \Theta(\omega_D - |i\omega_n|); \quad (6)$$

see Appendix C. Here, we have introduced a phenomenological Debye frequency  $\omega_D$  to model conventional, phonon-mediated pairing. The superconducting instability now corresponds to the condition  $\chi_0 = D_S/U$ .

If  $g_{\mathbf{k},i\omega_n}$  were the electron Green's function in a conventional metal, its only nonanalyticity would have been simple poles on the real axis. For the surface of a Weyl semimetal, the Green's function also has branch cuts on the real axis, so the Matsubara sum must be done with greater care. We carry out this exercise for an explicit model below. Nonetheless, the branch cuts do not change the result qualitatively in meaningful limits.

## III. TRACTABLE LAYERED MODEL

We consider a minimal model consisting of alternating layers of spinful electron and hole metals with dispersion

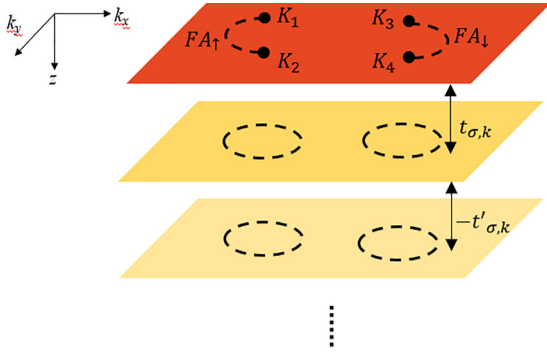


FIG. 3. Minimal layered model of a time-reversal symmetric Weyl semimetal showing two Fermi arcs with opposite spins.

$\pm \xi_{\sigma, \mathbf{k}} - \mu$  stacked along  $z$  and alternating, real interlayer couplings  $t_{\sigma, \mathbf{k}}, -t'_{\sigma, \mathbf{k}}$  [Fig. 3]. Its second-quantized Hamiltonian for an  $L$ -layered slab is given by

$$H = \int_{\mathbf{k}} \sum_{z=0}^{L-1} \sum_{\sigma=\uparrow, \downarrow} [(-1)^z \xi_{\sigma, \mathbf{k}} - \mu] c_{\sigma, \mathbf{k}, z}^{\dagger} c_{\sigma, \mathbf{k}, z} + \left[ \cos^2\left(\frac{\pi z}{2}\right) t_{\sigma, \mathbf{k}} - \sin^2\left(\frac{\pi z}{2}\right) t'_{\sigma, \mathbf{k}} \right] c_{\sigma, \mathbf{k}, z}^{\dagger} c_{\sigma, \mathbf{k}, z+1} + \text{H.c.}, \quad (7)$$

where  $c_{\sigma, \mathbf{k}, z}^{\dagger}$  creates an electron with spin  $\sigma$  at layer  $z$  and 2D momentum  $\mathbf{k} = (k_x, k_y)$ . The model clearly conserves spin and has two layers in each unit cell. Its bulk Bloch Hamiltonian in the bilayer basis in the  $\sigma$  sector is

$$H_{\sigma, \mathbf{k}} = \begin{pmatrix} \xi_{\sigma, \mathbf{k}} - \mu & t_{\sigma, \mathbf{k}} - t'_{\sigma, \mathbf{k}} e^{-2ik_z c} \\ t_{\sigma, \mathbf{k}} - t'_{\sigma, \mathbf{k}} e^{2ik_z c} & -\xi_{\sigma, \mathbf{k}} - \mu \end{pmatrix}, \quad (8)$$

where  $c$  is the interlayer spacing, assumed constant within and between unit cells for simplicity. The interlayer terms are phenomenologically chosen to produce Fermi arcs on the  $z = 0$  surface along  $\xi_{\sigma, \mathbf{k}} = \mu$  when  $t_{\sigma, \mathbf{k}}^2 < t'_{\sigma, \mathbf{k}}^2$  [Fig. 4]. This results in bulk Weyl nodes in the  $k_z = 0$  plane whenever  $t_{\sigma, \mathbf{k}} = t'_{\sigma, \mathbf{k}}$ . Near the  $j$ th Weyl node in the  $\sigma$  sector, at  $(\mathbf{k}, k_z) = (\mathbf{K}_{\sigma, j}, 0)$ , the low energy Hamiltonian can be written as

$$H_{\sigma, j}^{\text{Weyl}} = (\mathbf{v}_{\sigma, j} \cdot \mathbf{p}) \tau_z + (\mathbf{u}_{\sigma, j} \cdot \mathbf{p}) \tau_x + (w_{\sigma, j} p_z) \tau_y - \mu, \quad (9)$$

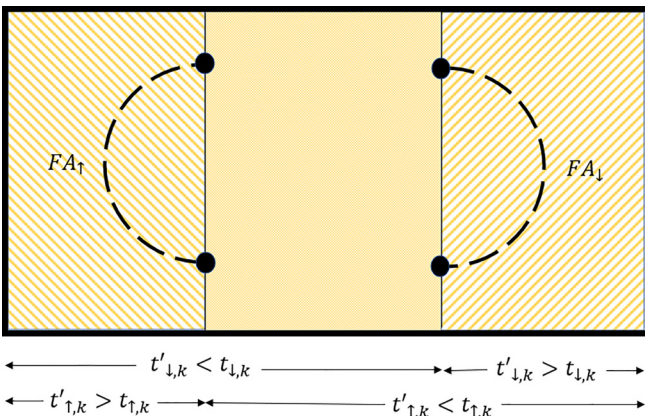


FIG. 4. Surface layer of Weyl semimetal with Fermi arcs. The Fermi arcs form when  $t'_{\sigma, \mathbf{k}} > t_{\sigma, \mathbf{k}}$  and  $\xi_{\sigma, \mathbf{k}} = 0$ .

where  $\tau_i$  are Pauli matrices in the bilayer basis;  $(\mathbf{p}, p_z)$  is the 3D momentum relative to the Weyl node; and  $\mathbf{v}_{\sigma, j} = \nabla_{\mathbf{k}} \xi_{\sigma, \mathbf{k}}|_{\mathbf{k}=\mathbf{K}_{\sigma, j}}$ ,  $\mathbf{u}_{\sigma, j} = \nabla_{\mathbf{k}} (t_{\sigma, \mathbf{k}} - t'_{\sigma, \mathbf{k}})|_{\mathbf{k}=\mathbf{K}_{\sigma, j}}$ , and  $w_{\sigma, j} = -2t'_{\sigma, \mathbf{K}_{\sigma, j}} c$  are Weyl velocities.

For this model,  $g_{\mathbf{k}, i\omega_n}$  can be calculated analytically in the semi-infinite limit,  $L \rightarrow \infty$ , following [75]. It is a  $2 \times 2$  diagonal matrix in the spin basis given by

$$g_{\sigma\sigma', \mathbf{k}, i\omega_n} = \delta_{\sigma\sigma'} \frac{a_{\sigma, \mathbf{k}, i\omega_n} + \sqrt{b_{\sigma, \mathbf{k}, i\omega_n}^+ b_{\sigma, \mathbf{k}, i\omega_n}^-}}{2t_{\sigma, \mathbf{k}}^2 (i\omega_n + \mu - \xi_{\sigma, \mathbf{k}})}, \quad (10)$$

$$a_{\sigma, \mathbf{k}, i\omega_n} = (i\omega_n + \mu)^2 - \xi_{\sigma, \mathbf{k}}^2 - t_{\sigma, \mathbf{k}}^2 + t_{\sigma, \mathbf{k}}'^2,$$

$$b_{\sigma, \mathbf{k}, i\omega_n}^{\pm} = (i\omega_n + \mu)^2 - E_{\sigma, \mathbf{k}}^{\pm 2},$$

$$E_{\sigma, \mathbf{k}}^{\pm} = \sqrt{\xi_{\sigma, \mathbf{k}}^2 + (t_{\sigma, \mathbf{k}} \pm t'_{\sigma, \mathbf{k}})^2}. \quad (11)$$

$g_{\mathbf{k}, \omega}$  has nonanalyticities on the real frequency axis in the form of poles at  $\omega = \xi_{\sigma, \mathbf{k}} - \mu$  that represent the Fermi arcs when  $\omega = 0$ , and a pair of square root branch cuts defined by  $E_{\sigma, \mathbf{k}}^- < |\omega + \mu| < E_{\sigma, \mathbf{k}}^+$  that corresponds to  $\omega$  being inside the bulk conduction and valence bands and capture the projection of these bands onto the surface. Along  $\xi_{\sigma, \mathbf{k}} = \mu$ , the surface also carries Luttinger arcs, defined as zeros of  $\det(g_{\mathbf{k}, 0})$ , which form closed loops with the Fermi arcs when  $\mu = 0$  [92].

This model is a variant of the spinless model introduced in Ref. [75]. Here, we assume two decoupled copies of the model, one for each spin, and ensure time-reversal symmetry by requiring  $t_{\sigma, \mathbf{k}}, t'_{\sigma, \mathbf{k}}$ , and  $\xi_{\sigma, \mathbf{k}}$  to be unchanged under the simultaneous reversal of spin and momentum,  $\sigma \rightarrow -\sigma, \mathbf{k} \rightarrow -\mathbf{k}$ . It contains a single orbital degree of freedom in each layer,  $D_z = 1 \forall z$ , so we will suppress the index  $n_z$  henceforth. We also suppress the spin index below for brevity and assume all functions to be the ones for spin-up, i.e.,  $\xi_{\mathbf{k}} \equiv \xi_{\sigma, \mathbf{k}}$ , etc.

#### IV. SURFACE INSTABILITY

We now use the above Green's function to evaluate  $\chi_0$  in Eq. (6) to obtain the instability. The trace over spin simply gives a factor of two. The pair of Green's functions yields two poles, at  $\omega = \xi_{\mathbf{k}+\mathbf{K}/2} - \mu, -\xi_{\mathbf{k}-\mathbf{K}/2} + \mu$ , and four branch cuts, defined by  $E_{\mathbf{k}+\mathbf{K}/2}^- < |\pm \omega + \mu| < E_{\mathbf{k}+\mathbf{K}/2}^+$ . Branch cuts from one Green's function factor can overlap with poles and branch cuts from the other, so the frequency integrals must be performed carefully. Summing over Matsubara frequencies gives separate contributions from the poles and branch cuts of  $g_{\mathbf{k}, \omega}$ ,  $\chi_0 = \chi_{\text{FA}} + \chi_{\text{proj}}$ .

##### A. Fermi arc contribution

The first contribution is

$$\chi_{\text{FA}} = \int_{\mathbf{k}} \tanh\left(\frac{\xi_{\mathbf{k}} - \mu}{2T}\right) R\left(1 - \frac{t_{\mathbf{k}}^2}{t_{\mathbf{k}}'^2}\right) \frac{\Theta(\omega_D - |\xi_{\mathbf{k}} - \mu|)}{\xi_{\mathbf{k}} - \mu} \times \frac{t_{\mathbf{k}}'^2 - t_{\mathbf{k}}^2 + 4\mu(\mu - \xi_{\mathbf{k}}) + \sqrt{\prod_{\lambda=\pm} (2\mu - \xi_{\mathbf{k}})^2 - (E_{\mathbf{k}}^{\lambda})^2}}{2t_{\mathbf{k}}'^2}, \quad (12)$$

where  $R(x) = (x + |x|)/2$  is the ramp function. For  $\omega_D$  much less than the hopping energy scales, it is useful to work in

momentum coordinates  $(k_{\parallel}, k_{\perp})$  parallel and perpendicular to the contour  $\xi_{\mathbf{k}} = \mu$ . Near this contour, we can approximate  $\xi_{\mathbf{k}} = \mu + v_{k_{\parallel}} k_{\perp}$ . This turns the above expression into a sum of integrals around each Fermi arc,  $\chi_{FA} = \sum_i \chi_{FA_i}$ , with

$$\chi_{FA_i} \approx \int_{k_{\parallel} \in FA_i} R^2 \left(1 - \frac{t_{k_{\parallel}}^2}{t_{k_{\parallel}}'^2}\right) \int_{|k_{\perp}| < \frac{\omega_D}{|v_{k_{\parallel}}|}} \frac{\tanh[v_{k_{\parallel}} k_{\perp}/2T]}{v_{k_{\parallel}} k_{\perp}}. \quad (13)$$

For  $\omega_D \gg T$ , the  $k_{\perp}$  integral is dominated by the region  $2T < |v_{k_{\parallel}} k_{\perp}| < \omega_D$ , where  $|\tanh[v_{k_{\parallel}} k_{\perp}/2T]| \approx 1$  and evaluates to  $(1/\pi |v_{k_{\parallel}}|) \ln(\omega_D/2T)$ . As a result,

$$\begin{aligned} \chi_{FA_i} &\approx \ln\left(\frac{\omega_D}{2T}\right) \int_{k_{\parallel} \in FA_i} \frac{1}{\pi |v_{k_{\parallel}}|} R^2 \left(1 - \frac{t_{k_{\parallel}}^2}{t_{k_{\parallel}}'^2}\right), \\ &\approx \frac{l_{FA_i}}{2\pi^2} \ln\left(\frac{\omega_D}{2T}\right) \left\langle \frac{1}{|v|} \right\rangle_{FA_i}, \end{aligned} \quad (14)$$

where  $l_{FA_i}$  is the length of the  $i$ th Fermi arc and  $\langle \dots \rangle_{FA_i}$  denotes a weighted average over this Fermi arc with  $k_{\parallel}$  dependent weight  $R^2(1 - t_{k_{\parallel}}^2/t_{k_{\parallel}}'^2)$ . Equation (14) matches the corresponding result for a 2D metal if  $l_{FA_i}$  is replaced by the perimeter of the Fermi surface and the weight is  $k_{\parallel}$  independent. Thus, Fermi arcs behave like a metallic Fermi surface for harbouring a Cooper instability.

### B. Contribution from bulk states

Next, we evaluate  $\chi_{\text{proj}}$ , the contribution to  $\chi_0$  from the projection of the bulk states onto the surface, captured by the branch cuts in  $g_{\mathbf{k}, \pm\omega}$ . Explicitly, we find

$$\begin{aligned} \chi_{\text{proj}} &= -2 \int_{\mathbf{k}} \int_{\omega \in \text{BC}} \tanh\left(\frac{\omega}{2T}\right) \sqrt{|b_{\mathbf{k},\omega}^+ b_{\mathbf{k},\omega}^-|} \text{sgn}(\omega + \mu) \\ &\quad \times \frac{a_{-\omega} + \sqrt{R[b_{\mathbf{k},-\omega}^+ b_{\mathbf{k},-\omega}^-]}}{t_{\mathbf{k}}'^4 [\omega^2 - (\mu - \xi_{\mathbf{k}})^2]} \Theta(\omega_D - |\omega|), \end{aligned} \quad (15)$$

where  $\omega \in \text{BC}$  denotes the branch cut region  $E_{\mathbf{k}}^- < |\omega + \mu| < E_{\mathbf{k}}^+$  and the factor of  $\text{sgn}(\omega + \mu)$  comes from selecting the principal values of the square roots.

In the regime,  $\omega_D \ll E_{\mathbf{k}}^+$ , the conditions  $\pm\omega \in \text{BC}$  reduce to  $E_{\mathbf{k}}^- < |\pm\omega + \mu|$ . Physically, this ensures that  $\chi_{\text{proj}}$  receives contributions only from  $\mathbf{k}$ -space regions defined by surface projections of bulk Fermi surfaces enclosing the Weyl nodes. Hence, we can linearize around the Weyl points as  $\xi_{\mathbf{p}} \approx \mathbf{v}_j \cdot \mathbf{p}$ ,  $t_{\mathbf{p}} \approx t_j + \mathbf{u}_j \cdot \mathbf{p}/2$  and  $t_{\mathbf{p}}' \approx t_j - \mathbf{u}_j \cdot \mathbf{p}/2$ . Then,  $E_{\mathbf{k}}^- \approx \sqrt{(\mathbf{v}_j \cdot \mathbf{p})^2 + (\mathbf{u}_j \cdot \mathbf{p})^2} \equiv \epsilon_{\mathbf{p}}$ ,  $a_{\mathbf{k},\omega} \approx -2t_j \mathbf{u}_j \cdot \mathbf{p}$ ,  $b_{\mathbf{k},\omega}^- \approx (\omega + \mu)^2 - \epsilon_{\mathbf{p}}^2$  and  $b_{\mathbf{k},\omega}^+ \approx -4t_j^2$  near the  $j$ th node.  $\chi_{\text{proj}}$  can then be written as  $\chi_{\text{proj}} = \sum_j \chi_{\text{proj},j}$  where

$$\begin{aligned} \chi_j^{\text{proj}} &\approx \frac{2}{\pi t_j^2} \int_0^{\omega_D} d\omega \tanh\left(\frac{\omega}{2T}\right) \int_{|\omega - |\mu|| < \epsilon_{\mathbf{p}} < \omega + |\mu|} \\ &\quad \times \frac{\sqrt{[(\omega + |\mu|)^2 - \epsilon_{\mathbf{p}}^2][\epsilon_{\mathbf{p}}^2 - (\omega - |\mu|)^2]}}{(|\mu| - \mathbf{v}_j \cdot \mathbf{p})^2 - \omega^2}. \end{aligned} \quad (16)$$

The pseudorelativistic form of  $\epsilon_{\mathbf{p}}$  makes the  $\mathbf{p}$  integral analytically tractable but rather unwieldy. The complications can be avoided by assuming  $\mathbf{u}_j \perp \mathbf{v}_j$  at the cost of  $O(1)$  prefactors.

Under this assumption,

$$\begin{aligned} \chi_j^{\text{proj}} &\approx \frac{8|\mu|^{3/2}}{3\pi^2 t_j^2 |u_j v_j|} \int_0^{\omega_D} d\omega \tanh\left(\frac{\omega}{2T}\right) \sqrt{\omega}, \\ &\approx \left(\frac{4}{3\pi t_j}\right)^2 \frac{|\mu|^{3/2} \omega_D^{3/2}}{|u_j v_j|}. \end{aligned} \quad (17)$$

Importantly, this is a small number compared to  $\chi_{FA}$  as it is suppressed by powers of  $\mu/t_j$  and  $\omega_D/t_j$ . Thus,  $\chi_0 \approx \chi_{FA}$ , and the surface instability is determined mainly by the FAs and resembles that of an ordinary 2D metal. The transition temperature follows from setting  $\chi_0 = 1/U$ . Explicitly,

$$T_C^{\text{surf}} \approx \frac{\omega_D}{2} \exp\left[-\frac{2\pi^2}{UV_{\text{cell}}^{2D} \sum_i l_{FA_i} \langle \frac{1}{|v|} \rangle_{FA_i}}\right], \quad (18)$$

where we have reinstated  $V_{\text{cell}}^{2D}$ . Strictly speaking, this is expected to be a Berzinskii-Kosterlitz-Thouless transition rather than a true superconducting transition. This is because the main role of the FAs is to contribute a 2D density of states to enable an instability, and their topological nature are essentially irrelevant.

## V. BULK INSTABILITY

We now study the superconducting instability in the bulk. We begin with the Hamiltonian near a Weyl node, Eq. (9), and compute the appropriate susceptibility  $\chi_{\text{bulk}}$  following the procedure described in Sec. II. We continue to suppress the spin index to avoid notational clutter, use spin-up functions only (e.g.,  $\xi_{\mathbf{k}} \equiv \xi_{\sigma,\mathbf{k}}$  etc.), and note that the spin sum merely contributes a factor of two to  $\chi_{\text{bulk}}$ . See Appendix D for details.

The Green's function near the  $j$ th Weyl node is

$$G_{j,\mathbf{p},i\omega_n} = \frac{1}{i\omega_n + \mu - \mathbf{v}_j \cdot \mathbf{p} \tau_z - \mathbf{u}_j \cdot \mathbf{p} \tau_x - w_j p_z \tau_y}. \quad (19)$$

Thus,  $\chi_{\text{bulk},j} = 2T \sum_{i\omega_n} \int_{\mathbf{p}} \text{Tr}[G_{j,\mathbf{p},i\omega_n}^T G_{j,\mathbf{p},-i\omega_n}] \Theta(\omega_D - |i\omega_n|)$  is given by

$$\begin{aligned} \chi_j^{\text{bulk}} &= 2T \sum_{i\omega_n} \Theta(\omega_D - |i\omega_n|) \\ &\quad \times \int_{\mathbf{p}} \frac{\mu^2 - (i\omega_n)^2 + \epsilon_{\mathbf{p},p_z}^2 - 2(w_j p_z)^2}{\prod_{s=\pm} [(i\omega_n + s\mu)^2 - \epsilon_{\mathbf{p},p_z}^2]}, \end{aligned} \quad (20)$$

where  $\epsilon_{\mathbf{p},p_z} = \sqrt{\epsilon_{\mathbf{p}}^2 + (w_j p_z)^2}$  is the pseudorelativistic dispersion near the Weyl node. Once again, the integrals are analytically tractable in this limit and yield  $\chi^{\text{bulk}} = \sum_j \chi_j^{\text{bulk}}$  with

$$\chi_j^{\text{bulk}} \approx \frac{\mu^2}{3\pi^2 |(\mathbf{u}_j \times \mathbf{v}_j) \cdot \mathbf{w}_j|} \ln\left(\frac{\omega_D}{2T}\right), \quad (21)$$

for  $\omega_D \gg T$ .

Readding  $V_{\text{cell}}^{3D}$  back into the expression, the bulk transition temperature is given by

$$T_C^{\text{bulk}} \approx \frac{\omega_D}{2} \exp\left[-\frac{3\pi^2}{UV_{\text{cell}}^{3D} \mu^2 \sum_j \frac{1}{|(\mathbf{u}_j \times \mathbf{v}_j) \cdot \mathbf{w}_j|}}\right]. \quad (22)$$

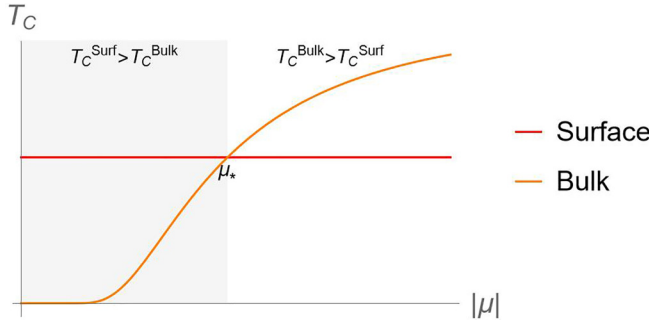


FIG. 5. Illustration of the parametric regime where the surface is superconducting while the bulk is in the normal phase.  $T_C^{\text{surf}}$  is expected to depend weakly on  $\mu$  while  $T_C^{\text{bulk}} \sim e^{-1/\mu^2}$ . For  $|\mu| < \mu_*$ ,  $T_C^{\text{bulk}} < T_C^{\text{surf}}$ , so  $T$  between these critical values will see surface-only superconductivity.

Naturally,  $T_C^{\text{bulk}} \rightarrow 0$  as  $\mu = 0$  and grows smoothly with  $\mu$ . Crucially, there exists a parametrically large regime in which  $T_C^{\text{bulk}} < T_C^{\text{surf}}$ , namely when  $|\mu| < \mu_*$ , where

$$\mu_*^2 = \hbar^2 \frac{3V_{\text{cell}}^{2D} \sum_i l_{\text{FA}_i} \left( \frac{1}{|v|} \right)_{\text{FA}_i}}{2V_{\text{cell}}^{3D} \sum_j \frac{1}{|(\mathbf{u}_j \times \mathbf{v}_j) \cdot \mathbf{w}_j|}}. \quad (23)$$

In this regime, the surface will superconduct while the bulk will remain metallic (see Fig. 5) with the caveat that the surface superconductivity will presumably be of the Berezinskii-Kosterlitz-Thouless type. We have assumed the same  $\mu$  relative to the Weyl node for each node, i.e.,  $\mu_j = \mu \forall j$ . In real materials, Weyl nodes not related by symmetry occur at different energies. Then, the appropriate condition for  $T_C^{\text{bulk}} < T_C^{\text{surf}}$  is  $\mu_{\text{max}} = \max_j |\mu_j| < \mu_*$ . Intuitively, this is the condition that the bulk density of states is smaller than the surface density of states after appropriate scaling by the unit cell volume in each dimension. Thus, surface-only superconductivity can occur in principle even if the bulk contains trivial Fermi surfaces, provided they are small enough. Estimating realistic parameters, i.e.,  $l_{\text{FA}} \sim 10^{10}$  m,  $|v_{\text{FA}}| \sim 10^3$  m/s,  $V_{\text{cell}}^{2D} \sim 10^{-18}$  m<sup>2</sup>,  $V_{\text{cell}}^{3D} \sim 10^{-27}$  m<sup>3</sup>, and  $|(\mathbf{u}_j \times \mathbf{v}_j) \cdot \mathbf{w}_j| \sim 10^{12}$  m<sup>3</sup>/s<sup>3</sup>, we estimate  $\mu_* \sim 10^{-2}$  eV.

## VI. EXPERIMENTAL RELEVANCE

This result is pertinent to the observations of superconductivity in t-PtBi<sub>2</sub>. In particular, Schimmel *et al.* saw a wide range of surface superconducting gaps in the tunneling spectrum of t-PtBi<sub>2</sub>, with the largest gaps corresponding to  $T_C \sim 100$  K range [57]. In comparison, transport measurements in bulk crystals and thin films displayed  $T_C \sim 0.6$  K [56] and  $T_C \sim 0.275$ – $0.400$  [69], respectively. The latter saw a Berezinskii-Kosterlitz-Thouless transition in films up to 60 nm thick whereas such a transition is expected only in 2D superconductors, typically no more than a few nm in thickness. In a similar vein, Kuibarov *et al.* using ARPES inferred a surface  $T_C$  of  $14 \pm 2$  K and  $8 \pm 2$  K for the two surface terminations [70] where the bulk was inferred to be in a normal state. The authors of Ref. [57] speculated that the higher  $T_C$  on the surface was due to a transition from bulk to surface superconductivity and asked whether the surface superconductivity is connected to the topologically nontrivial

states found on the surface of a type-I Weyl semimetal. We have shown, in a toy model, that the dominant part of surface superconductivity indeed emerges from FA states and yields a higher  $T_C$  on the surface than in the bulk. Moreover, we argued that the surface superconductivity is essentially 2D and should exhibit a Berezinskii-Kosterlitz-Thouless transition.

Our work is also relevant to the observation of superconductivity with  $T_C$  of 6 K–9 K in powdered samples of NbP, a type-I Weyl semimetal, by Baenitz *et al.* [47]. This was in agreement with another published value,  $T_C \sim 7.5$  K [46], for powdered NbP compounds. Baenitz *et al.* reported a superconducting fraction of only 6.2% and gave two possible explanations based on grain size effects for the small fraction. The first one involved strain on the grains, turning the material into a type-II Weyl semimetal, which has a bigger Fermi surface and is thus more likely to superconduct. The second explanation involved superconductivity developing on the surface, which can lead to a sizable signature in powder samples. We have shown that the second latter picture is possible, at least within mean-field theory in a phenomenological model. Moreover, we note that in the first picture, different samples would likely turn into type-II Weyl semimetals with differing sizes of electron and hole pockets and exhibit vastly different  $T_C$ , unlike what was observed. In contrast, intrinsic surface superconductivity is more likely to yield similar transition temperatures in different samples. Our picture can be tested by studying superconductivity in bulk and thin films of NbP. If superconductivity intrinsically occurred on the surface, thin films would display a larger superconducting fraction than bulk crystals in sharp contrast to the behavior of conventional metallic superconductors.

## VII. SUMMARY

We have shown that under a mean-field limit in a phenomenological model of a TWSM, there exists a parametrically large regime where the surface has a superconducting instability, whereas the bulk remains in the normal state. Furthermore, we find that the instability is governed mainly by the Fermi arc surface states, and the contribution from the surface projection of the bulk Fermi surface is negligible. This result pertains to recent experiments on NbP and t-PtBi<sub>2</sub> that raised the possibility of intrinsic surface superconductivity in TWSMs.

## ACKNOWLEDGMENTS

We acknowledge financial support from the National Science Foundation, Grant No. DMR 2047193. We are grateful to Kai Chen and Osakpolor Obakpolor for useful discussions.

## APPENDIX A: SURFACE GREEN'S FUNCTION

Let  $H_{\mathbf{k}}^B$  denote the Bloch Hamiltonian of an  $L$ -layered time-reversal symmetric system that has  $2D_z$  degrees of freedom in the  $z$ th layer. Time-reversal symmetry (TRS) ensures that each layer has an even number of degrees of freedom. The layers are unrelated in general but repeat periodically in lattice models. Now, let us add a layer at  $z = 0$  that we refer to as the

“surface.” The Hamiltonian for the full system is of the form

$$H_{\mathbf{k}} = \begin{pmatrix} H_{\mathbf{k}}^S & h_{\mathbf{k}} \\ h_{\mathbf{k}}^\dagger & H_{\mathbf{k}}^B \end{pmatrix}. \quad (\text{A1})$$

We will use  $\bar{b}, b$  to denote Grassman variables for fermions in layers  $1, \dots, L$ , and  $\bar{s}, s$  for surface fermions. Contractions over layers ( $z$ ), orbitals ( $n_z$ ), and spin ( $\sigma$ ) will be denoted by “.” while integrals will be written in shorthand as  $\int_{\mathbf{k}, \tau} \equiv \int_0^\beta d\tau \int \frac{d^2k}{(2\pi)^2}$ . In this notation, the Euclidean path integrals for the  $L$ - and  $(L+1)$ -layered systems are  $Z_0^B = \int \mathcal{D}[\bar{b}, b] \exp[-S_0^B(\bar{b}, b)]$  and  $Z_0 = \int \mathcal{D}[\bar{b}, b, \bar{s}, s] \exp[-S_0(\bar{b}, b, \bar{s}, s)]$ , where

$$S_0(\bar{b}, b) = - \int_{\mathbf{k}, \tau} \sum_{z, z'=1}^L \sum_{\sigma, \sigma' \in \uparrow, \downarrow} \bar{b}_{\mathbf{k}, z, n_z, \sigma} (\partial_\tau \delta_{(z, n_z, \sigma), (z', n_{z'}, \sigma')}) + H_{\mathbf{k}, (z, n_z, \sigma), (z', n_{z'}, \sigma')}^B b_{\mathbf{k}, z', n_{z'}, \sigma'}, \quad (\text{A2})$$

$$\equiv \int_{\mathbf{k}, \tau} \bar{b}_{\mathbf{k}} \cdot [G_{\mathbf{k}}^B(\tau)]^{-1} \cdot b_{\mathbf{k}}, \quad (\text{A3})$$

$$S_0(\bar{b}, b, \bar{s}, s) = - \int_{\mathbf{k}, \tau} (\bar{s}_{\mathbf{k}}, \bar{b}_{\mathbf{k}}) \cdot (\partial_\tau + H_{\mathbf{k}}) \cdot \begin{pmatrix} s_{\mathbf{k}} \\ b_{\mathbf{k}} \end{pmatrix}, \quad (\text{A4})$$

$$\equiv \int_{\mathbf{k}, \tau} (\bar{s}_{\mathbf{k}}, \bar{b}_{\mathbf{k}}) \cdot [G_{\mathbf{k}}(\tau)]^{-1} \cdot \begin{pmatrix} s_{\mathbf{k}} \\ b_{\mathbf{k}} \end{pmatrix}. \quad (\text{A5})$$

We have introduced imaginary time Green's functions  $G_{\mathbf{k}}^B(\tau)$  and  $G_{\mathbf{k}}(\tau)$  for the  $L$ - and  $(L+1)$ -layered system. Integrating out the  $b$  fermions yields an effective surface Green's function  $g_{\mathbf{k}}(\tau)$  as follows:

$$Z_0^S = \frac{Z_0}{Z_0^B} \equiv \int \mathcal{D}[\bar{s}, s] \exp[-S_0^S(\bar{s}, s)], \quad (\text{A6})$$

$$S_0^S(\bar{s}, s) = - \int_{\mathbf{k}, \tau} \bar{s}_{\mathbf{k}} \cdot [\partial_\tau + H_{\mathbf{k}}^S + h_{\mathbf{k}} G_{\mathbf{k}}^B(\tau) h_{\mathbf{k}}^\dagger] \cdot s_{\mathbf{k}}, \quad (\text{A7})$$

$$\Rightarrow g_{\mathbf{k}}(\tau) = -(\partial_\tau + H_{\mathbf{k}}^S + h_{\mathbf{k}} G_{\mathbf{k}}^B(\tau) h_{\mathbf{k}}^\dagger)^{-1}. \quad (\text{A8})$$

The Matsubara Green's functions  $G_{\mathbf{k}}^B(i\omega_n)$ ,  $G_{\mathbf{k}}(i\omega_n)$ , and  $g_{\mathbf{k}}(i\omega_n)$  can be obtained straightforwardly by the replacement  $\partial_\tau \rightarrow -i\omega_n$  in the above equations.

## APPENDIX B: INTERACTION

Since the interaction is local, the path integral for the full interacting system factorizes between the bulk and the surface:  $Z = Z^B Z^S$ , where

$$Z^B = \int \mathcal{D}[\bar{b}, b] \exp[-S_0^B(\bar{b}, b) - S_{int}^B(\bar{b}, b)], \quad (\text{B1})$$

$$S_{int}^B(\bar{b}, b) = - \int_{\mathbf{k}, \tau} \sum_z \frac{U}{D_z} \bar{\mathbb{B}}_{\mathbf{k}, z} \mathbb{B}_{\mathbf{k}, z}, \quad (\text{B2})$$

$$\mathbb{B}_{\mathbf{k}, z} = \sum_{n_z=1}^{D_z} \int_{\mathbf{k}} b_{\frac{\mathbf{k}}{2} + \mathbf{k}, z, n_z, \downarrow} b_{\frac{\mathbf{k}}{2} - \mathbf{k}, z, n_z, \uparrow}, \quad (\text{B3})$$

and

$$Z^S = \int \mathcal{D}[\bar{s}, s] \exp[-S_0^S(\bar{s}, s) - S_{int}^S(\bar{s}, s)], \quad (\text{B4})$$

$$S_{int}^S(\bar{s}, s) = - \frac{U}{D_S} \int_{\mathbf{k}, \tau} \bar{\mathbb{S}}_{\mathbf{k}} \mathbb{S}_{\mathbf{k}}, \quad (\text{B5})$$

$$\mathbb{S}_{\mathbf{k}} = \sum_{n_S=1}^{D_S} \int_{\mathbf{k}} s_{\frac{\mathbf{k}}{2} + \mathbf{k}, n_S, \downarrow} s_{\frac{\mathbf{k}}{2} - \mathbf{k}, n_S, \uparrow}. \quad (\text{B6})$$

The fermion bilinears  $\mathbb{B}_{\mathbf{k}, z}$  and  $\mathbb{S}_{\mathbf{k}}$  are bosonic variables, and  $D_S \equiv D_0$  is the number of degrees of freedom in the  $z=0$  surface layer.

To investigate surface superconductivity, we focus on  $Z^S$ . Decoupling the interaction term in the  $s$ -wave pairing channel through another bosonic field  $\Delta_{2\mathbf{K}}$  gives

$$Z^S = \int \mathcal{D}[\bar{s}, s] \exp[-S_0^S(\bar{s}, s)] \times \int \mathcal{D}[\bar{\Delta}, \Delta] \exp[-S'(\bar{\Delta}, \Delta, \bar{s}, s)], \quad (\text{B7})$$

where

$$S'(\bar{\Delta}, \Delta, \bar{s}, s) = \int_{\mathbf{K}, \tau} - \frac{D_S}{U} \bar{\Delta}_{\mathbf{K}} \Delta_{\mathbf{K}} + \bar{\mathbb{S}}_{\mathbf{K}} \Delta_{\mathbf{K}} + \bar{\Delta}_{\mathbf{K}} \mathbb{S}_{\mathbf{K}}. \quad (\text{B8})$$

## APPENDIX C: GREEN'S FUNCTION TRACE

In this section, we show how the expressions for  $\chi_0$  can be simplified and written as the trace of a product of Green's functions:

$$\chi_0 = \int_{\mathbf{k}, i\omega_n} [g_{\mathbf{k}}(i\omega_n)]_{nn'}^{\sigma\sigma'} [g_{-\mathbf{k}}(-i\omega_n)]_{nn'}^{\bar{\sigma}\bar{\sigma}'}, \quad (\text{C1})$$

$$= \int_{\mathbf{k}, i\omega_n} [g_{\mathbf{k}}(i\omega_n)]_{nn'}^{\sigma\sigma'} [\mathcal{T} g_{\mathbf{k}}(i\omega_n) \mathcal{T}^{-1}]_{nn'}^{\sigma\sigma'}, \quad (\text{C2})$$

$$= \int_{\mathbf{k}, i\omega_n} \text{tr}[g_{\mathbf{k}}^T(i\omega_n) \mathcal{T} g_{\mathbf{k}}(i\omega_n) \mathcal{T}^{-1}], \quad (\text{C3})$$

where the trace runs over both spin and orbital indices,  $\int_{\mathbf{k}, i\omega_n} = T \sum_{i\omega_n} \int \frac{d^2k}{(2\pi)^2}$  and  $\mathcal{T}$  denotes time reversal. We have used the action of  $\mathcal{T}$  on the matrix elements of  $g_{\mathbf{k}}(i\omega_n)$ :

$$[\mathcal{T} g_{\mathbf{k}}(i\omega_n) \mathcal{T}^{-1}]_{nn'}^{\sigma\sigma'} = [g_{-\mathbf{k}}(-i\omega_n)]_{nn'}^{\bar{\sigma}\bar{\sigma}'}, \quad (\text{C4})$$

and used the identity  $\text{tr}(AB^T) = \text{tr}(A^T B)$  to reduce notational clutter. Since the system is  $\mathcal{T}$  symmetric,  $\mathcal{T} g_{\mathbf{k}}(i\omega_n) \mathcal{T}^{-1} = g_{\mathbf{k}}(-i\omega_n)$ . This gives

$$\chi_0 = \int_{\mathbf{k}, i\omega_n} \text{tr}[g_{\mathbf{k}}^T(i\omega_n) g_{\mathbf{k}}(-i\omega_n)]. \quad (\text{C5})$$

Above, we separated the  $\sigma$  and  $n$  indices for clarity and assumed the orbitals to be  $\mathcal{T}$  symmetric. However, the expression in terms of  $\text{tr}(gg^T)$  should work even if the orbitals are not  $\mathcal{T}$  symmetric. In general,

$$\chi_{\mathbf{K}} = \int_{\mathbf{k}, i\omega_n} [g_{\mathbf{K}/2+\mathbf{k}}(i\omega_n)]_{n_S n'_S}^{\sigma\sigma'} [g_{\mathbf{K}/2-\mathbf{k}}(-i\omega_n)]_{n_S n'_S}^{\bar{\sigma}\bar{\sigma}'}, \quad (\text{C6})$$

$$= \int_{\mathbf{k}, i\omega_n} [g_{\mathbf{K}/2+\mathbf{k}}(i\omega_n)]_{n_S n'_S}^{\sigma\sigma'} [\mathcal{T} g_{-\mathbf{K}/2+\mathbf{k}}(i\omega_n) \mathcal{T}^{-1}]_{n_S n'_S}^{\sigma\sigma'}, \quad (\text{C7})$$

$$= \int_{\mathbf{k}, i\omega_n} \text{tr}[g_{\mathbf{K}+\mathbf{K}/2}^T(i\omega_n) g_{\mathbf{K}-\mathbf{K}/2}(-i\omega_n)]. \quad (\text{C8})$$

**APPENDIX D: INTEGRALS FOR CALCULATING  $\chi_{bulk}$** 

In this section, we describe the integration steps for computing  $\chi_{bulk}$ . We begin with Eq. (20) from the main text:

$$\chi_j^{bulk} = 2T \sum_{i\omega_n} \int_{\mathbf{p}} \frac{\mu^2 - (i\omega_n)^2 + \varepsilon_{\mathbf{p},p_z}^2 - 2(w_j p_z)^2}{\prod_{s=\pm} [(i\omega_n + s\mu)^2 - \varepsilon_{\mathbf{p},p_z}^2] \Theta(\omega_D - |i\omega_n|)}, \quad (\text{D1})$$

where  $\varepsilon_{\mathbf{p},p_z} = \sqrt{\varepsilon_{\mathbf{p}}^2 + (w_j p_z)^2}$  and  $\varepsilon_{\mathbf{p}} = \sqrt{(\mathbf{v}_j \cdot \mathbf{p})^2 + (\mathbf{u}_j \cdot \mathbf{p})^2}$  are massless relativistic dispersions in 3D and 2D. To bring the integrals into a spherically symmetric form, we rotate and rescale the momenta as

$$\begin{pmatrix} q_x \\ q_y \\ q_z \end{pmatrix} = \begin{pmatrix} V_j & 0 & 0 \\ 0 & U_j & 0 \\ 0 & 0 & w_j \end{pmatrix} \begin{pmatrix} \cos \theta_j & -\sin \theta_j & 0 \\ \sin \theta_j & \cos \theta_j & 0 \\ 0 & 0 & 1 \end{pmatrix} \begin{pmatrix} p_{\parallel} \\ p_{\perp} \\ p_z \end{pmatrix}. \quad (\text{D2})$$

This gives

$$\begin{aligned} \chi_j^{bulk} &= 2T \sum_{i\omega_n} \int \frac{d^3 q}{U_j V_j w_j (2\pi)^3} \frac{\mu^2 - (i\omega_n)^2 + q_x^2 + q_y^2 - q_z^2}{\prod_{s=\pm} [(i\omega_n + s\mu)^2 - q^2]} \Theta(\omega_D - |i\omega_n|), \\ &= \frac{1}{\pi^2 U_j V_j w_j} T \sum_{i\omega_n} \int_0^{\infty} q^2 dq \frac{\mu^2 - (i\omega_n)^2 + q^2/3}{[(i\omega_n + \mu)^2 - q^2][(i\omega_n - \mu)^2 - q^2]} \Theta(\omega_D - |i\omega_n|). \end{aligned} \quad (\text{D3})$$

Performing the Matsubara sum and some algebra gives

$$\chi_j^{bulk} = -\frac{1}{4\pi^2 U_j V_j w_j \mu} \int_{\mu - \omega_D}^{\mu + \omega_D} q^2 dq \frac{q/3 - \mu}{q - \mu} \tanh\left(\frac{q - \mu}{2T}\right). \quad (\text{D4})$$

Shifting  $q$  by  $\mu$  results in a symmetric integration range and causes several terms to vanish. We are then left with

$$\chi_j^{bulk} = \frac{\mu^2}{6\pi^2 U_j V_j w_j} \int_{-\omega_D}^{\omega_D} dq \frac{\tanh(q/2T)}{q}. \quad (\text{D5})$$

For  $\omega_D \gg T$ ,

$$\chi_j^{bulk} \approx \frac{\mu^2}{3\pi^2 |(\mathbf{u}_j \times \mathbf{v}_j) \cdot \mathbf{w}_j|} \left[ \ln\left(\frac{\omega_D}{2T}\right) + O(1) \right]. \quad (\text{D6})$$

- 
- [1] O. Vafeek and A. Vishwanath, Dirac fermions in solids: From high- $T_c$  cuprates and graphene to topological insulators and Weyl semimetals, *Annu. Rev. Condens. Matter Phys.* **5**, 83 (2014).
- [2] A. A. Burkov, Weyl Metals, *Annu. Rev. Condens. Matter Phys.* **9**, 359 (2018).
- [3] A. A. Burkov, Topological semimetals, *Nat. Mater.* **15**, 1145 (2016).
- [4] B. Yan and C. Felser, Topological materials: Weyl semimetals, *Annu. Rev. Condens. Matter Phys.* **8**, 337 (2017).
- [5] N. P. Armitage, E. J. Mele, and A. Vishwanath, Weyl and Dirac semimetals in three-dimensional solids, *Rev. Mod. Phys.* **90**, 015001 (2018).
- [6] S.-Q. Shen, Topological Dirac and Weyl semimetals (2017).
- [7] I. Belopolski, D. S. Sanchez, Y. Ishida, X. Pan, P. Yu, S.-Y. Xu, G. Chang, T.-R. Chang, H. Zheng, N. Alidoust, G. Bian, M. Neupane, S.-M. Huang, C.-C. Lee, Y. Song, H. Bu, G. Wang, S. Li, G. Eda, H.-T. Jeng *et al.*, Discovery of a new type of topological Weyl fermion semimetal state in  $\text{Mo}_x\text{W}_{1-x}\text{Te}_2$ , *Nat. Commun.* **7**, 13643 (2016).
- [8] Z. P. Guo, P. C. Lu, T. Chen, J. F. Wu, J. Sun, and D. Y. Xing, High-pressure phases of Weyl semimetals NbP, NbAs, TaP, and TaAs, *Sci. China Phys. Mech. Astron.* **61038211** (2018).
- [9] G. Chang, S.-Y. Xu, H. Zheng, C.-C. Lee, S.-M. Huang, I. Belopolski, D. S. Sanchez, G. Bian, N. Alidoust, T.-R. Chang, C.-H. Hsu, H.-T. Jeng, A. Bansil, H. Lin, and M. Z. Hasan, Signatures of Fermi arcs in the quasiparticle interferences of the Weyl semimetals TaAs and NbP, *Phys. Rev. Lett.* **116**, 066601 (2016).
- [10] A. Gyenis, H. Inoue, S. Jeon, B. B. Zhou, B. E. Feldman, Z. Wang, J. Li, S. Jiang, Q. D. Gibson, S. K. Kushwaha, J. W. Krizan, N. Ni, R. J. Cava, B. A. Bernevig, and A. Yazdani, Imaging electronic states on topological semimetals using scanning tunneling microscopy, *New J. Phys.* **18**, 105003 (2016).
- [11] S.-M. Huang, S.-Y. Xu, I. Belopolski, C.-C. Lee, G. Chang, B. Wang, N. Alidoust, G. Bian, M. Neupane, C. Zhang, S. Jia, A. Bansil, H. Lin, and M. Z. Hasan, A Weyl Fermion semimetal with surface Fermi arcs in the transition metal mononitride TaAs class, *Nat. Commun.* **6**, 7373 (2015).
- [12] H. Inoue, A. Gyenis, Z. Wang, J. Li, S. W. Oh, S. Jiang, N. Ni, B. A. Bernevig, and A. Yazdani, Quasiparticle interference of the Fermi arcs and surface-bulk connectivity of a Weyl semimetal, *Science* **351**, 1184 (2016).
- [13] B. Q. Lv, N. Xu, H. M. Weng, J. Z. Ma, P. Richard, X. C. Huang, L. X. Zhao, G. F. Chen, C. E. Matt, F. Bisti, V. N. Strocov, J. Mesot, Z. Fang, X. Dai, T. Qian, M. Shi, and H.

- Ding, Observation of Weyl nodes in TaAs, *Nat. Phys.* **11**, 724 (2015).
- [14] Y. Sun, S. C. Wu, and B. Yan, Topological surface states and Fermi arcs of the noncentrosymmetric Weyl semimetals TaAs, TaP, NbAs, and NbP, *Phys. Rev. B* **92**, 115428 (2015).
- [15] S.-Y. Xu, I. Belopolski, N. Alidoust, M. Neupane, G. Bian, C. Zhang, R. Sankar, G. Chang, Z. Yuan, C.-C. Lee, S.-M. Huang, H. Zheng, J. Ma, D. S. Sanchez, B. Wang, A. Bansil, F. Chou, P. P. Shibayev, H. Lin, S. Jia *et al.*, Discovery of a Weyl fermion semimetal and topological Fermi arcs, *Science* **349**, 613 (2015).
- [16] S. Y. Xu, I. Belopolski, D. S. Sanchez, M. Neupane, G. Chang, K. Yaji, Z. Yuan, C. Zhang, K. Kuroda, G. Bian, C. Guo, H. Lu, T. R. Chang, N. Alidoust, H. Zheng, C. C. Lee, S. M. Huang, C. H. Hsu, H. T. Jeng, A. Bansil *et al.*, Spin polarization and texture of the Fermi arcs in the Weyl fermion semimetal TaAs, *Phys. Rev. Lett.* **116**, 096801 (2016).
- [17] L. X. Yang, Z. K. Liu, Y. Sun, H. Peng, H. F. Yang, T. Zhang, B. Zhou, Y. Zhang, Y. F. Guo, M. Rahn, D. Prabhakaran, Z. Hussain, S. K. Mo, C. Felser, B. Yan, and Y. L. Chen, Weyl semimetal phase in the non-centrosymmetric compound TaAs, *Nat. Phys.* **11**, 728 (2015).
- [18] H. Zheng, S. Y. Xu, G. Bian, C. Guo, G. Chang, D. S. Sanchez, I. Belopolski, C. C. Lee, S. M. Huang, X. Zhang, R. Sankar, N. Alidoust, T. R. Chang, F. Wu, T. Neupert, F. Chou, H. T. Jeng, N. Yao, A. Bansil, S. Jia *et al.*, Atomic-scale visualization of quantum interference on a Weyl semimetal surface by scanning tunneling microscopy, *ACS Nano* **10**, 1378 (2016).
- [19] P. Hosur and X. Qi, Recent developments in transport phenomena in Weyl semimetals, *C. R. Phys.* **14**, 857 (2013).
- [20] H. Wang and J. Wang, Electron transport in Dirac and Weyl semimetals, *Chin. Phys. B* **27**, 107402 (2018).
- [21] J. Hu, S.-Y. Xu, N. Ni, and Z. Mao, Transport of topological semimetals, *Annu. Rev. Mater. Res.* **49**, 207 (2019).
- [22] A. A. Zyuzin and A. A. Burkov, Topological response in Weyl semimetals and the chiral anomaly, *Phys. Rev. B* **86**, 115133 (2012).
- [23] Y. Chen, S. Wu, and A. A. Burkov, Axion response in Weyl semimetals, *Phys. Rev. B* **88**, 125105 (2013).
- [24] M. M. Vazifeh and M. Franz, Electromagnetic response of Weyl semimetals, *Phys. Rev. Lett.* **111**, 027201 (2013).
- [25] A. A. Burkov, Chiral anomaly and transport in Weyl metals, *J. Phys.: Condens. Matter* **27**, 113201 (2015).
- [26] P. Hosur, S. Parameswaran, and A. Vishwanath, Charge Transport in Weyl Semimetals, *Phys. Rev. Lett.* **108**, 046602 (2012).
- [27] F. de Juan, A. G. Grushin, T. Morimoto, and J. E. Moore, Quantized circular photogalvanic effect in Weyl semimetals, *Nat. Commun.* **8**, 15995 (2017).
- [28] S. Wang, B. C. Lin, A. Q. Wang, D. P. Yu, and Z. M. Liao, Quantum transport in Dirac and Weyl semimetals: A review, *Adv. Phys.: X* **2**, 518 (2017).
- [29] K. Halterman, M. Alidoust, and A. Zyuzin, Epsilon-near-zero response and tunable perfect absorption in Weyl semimetals, *Phys. Rev. B* **98**, 085109 (2018).
- [30] K. Halterman and M. Alidoust, Waveguide modes in Weyl semimetals with tilted Dirac cones, *Opt. Express* **27**, 36164 (2019).
- [31] N. Nagaosa, T. Morimoto, and Y. Tokura, Transport, magnetic and optical properties of Weyl materials, *Nat. Rev. Mater.* **5**, 621 (2020).
- [32] H. B. Nielsen and M. Ninomiya, The Adler-Bell-Jackiw anomaly and Weyl fermions in a crystal, *Phys. Lett. B* **130**, 389 (1983).
- [33] M. V. Isachenkov and A. V. Sadofyev, The chiral magnetic effect in hydrodynamical approach, *Phys. Lett. B* **697**, 404 (2011).
- [34] A. V. Sadofyev, V. I. Shevchenko, and V. I. Zakharov, Notes on chiral hydrodynamics within the effective theory approach, *Phys. Rev. D* **83**, 105025 (2011).
- [35] R. Loganayagam and P. Surówka, Anomaly/transport in an Ideal Weyl gas, *J. High Energy Phys.* **04** (2012) 97.
- [36] P. Goswami and S. Tewari, Axionic field theory of (3+1)-dimensional Weyl semimetals, *Phys. Rev. B* **88**, 245107 (2013).
- [37] Z. Wang and S.-C. Zhang, Chiral anomaly, charge density waves, and axion strings from Weyl semimetals, *Phys. Rev. B* **87**, 161107 (2013).
- [38] G. Başar, D. E. Kharzeev, and H.-U. Yee, Triangle anomaly in Weyl semimetals, *Phys. Rev. B* **89**, 035142 (2014).
- [39] K. Landsteiner, Anomalous transport of Weyl fermions in Weyl semimetals, *Phys. Rev. B* **89**, 075124 (2014).
- [40] H. H. Wang, H. H. Wang, Y. Chen, J. Luo, Z. Yuan, J. Liu, Y. Wang, S. Jia, X.-J. Liu, J. Wei, and J. Wang, Discovery of tip induced unconventional superconductivity on Weyl semimetal, *Sci. Bull.* **62**, 425 (2017).
- [41] L. Aggarwal, S. Gayen, S. Das, R. Kumar, V. Süß, C. Felser, C. Shekhar, and G. Sheet, Mesoscopic superconductivity and high spin polarization coexisting at metallic point contacts on Weyl semimetal TaAs, *Nat. Commun.* **8**, 13974 (2017).
- [42] H. Wang, Y. He, Y. Liu, Z. Yuan, S. Jia, L. Ma, X.-J. Liu, and J. Wang, Ferromagnetic tip induced unconventional superconductivity in Weyl semimetal, *Sci. Bull.* **65**, 21 (2020).
- [43] J. Luo, Y. Li, J. Li, T. Hashimoto, T. Kawakami, H. Lu, S. Jia, M. Sato, and J. Wang, Surface superconductivity on Weyl semimetal induced by nonmagnetic and ferromagnetic tips, *Phys. Rev. Mater.* **3**, 124201 (2019).
- [44] Y. Li, Y. Zhou, Z. Guo, F. Han, X. Chen, P. Lu, X. Wang, C. An, Y. Zhou, J. Xing, G. Du, X. Zhu, H. Yang, J. Sun, Z. Yang, W. Yang, H.-K. Mao, Y. Zhang, and H.-H. Wen, Concurrence of superconductivity and structure transition in Weyl semimetal TaP under pressure, *npj Quantum Mater.* **2**, 66 (2017).
- [45] M. R. van Delft, S. Pezzini, M. König, P. Tinnemans, N. E. Hussey, and S. Wiedmann, Two- and Three-Dimensional Superconducting Phases in the Weyl Semimetal TaP at Ambient Pressure, *Crystals* **10**, 288 (2020).
- [46] P. Kumar, Sudesh, and S. Patnaik, Possible superconductivity in Weyl semimetal nbp, *AIP Conf. Proc.* **1731**, 140063 (2016).
- [47] M. Baenitz, M. Schmidt, V. Suess, C. Felser, and K. Lüders, Superconductivity in Weyl semimetal NbP: Bulk vs. surface, *J. Phys.: Conf. Ser.* **1293**, 012002 (2019).
- [48] D. Kang, Y. Zhou, W. Yi, C. Yang, J. Guo, Y. Shi, S. Zhang, Z. Wang, C. Zhang, S. Jiang, A. Li, K. Yang, Q. Wu, G. Zhang, L. Sun, and Z. Zhao, Superconductivity emerging from a suppressed large magnetoresistant state in tungsten ditelluride, *Nat. Commun.* **6**, 7804 (2015).
- [49] X.-C. Pan, X. Chen, H. Liu, Y. Feng, Z. Wei, Y. Zhou, Z. Chi, L. Pi, F. Yen, F. Song, X. Wan, Z. Yang, B. Wang, G. Wang, and Y. Zhang, Pressure-driven dome-shaped superconductivity and electronic structural evolution in tungsten ditelluride, *Nat. Commun.* **6**, 7805 (2015).

- [50] Y. Li, Q. Gu, C. Chen, J. Zhang, Q. Liu, X. Hu, J. Liu, Y. Liu, L. Ling, M. Tian, Y. Wang, N. Samarth, S. Li, T. Zhang, J. Feng, and J. Wang, Nontrivial superconductivity in topological  $\text{MoTe}_{2-x}\text{S}_x$  crystals, *Proc. Natl. Acad. Sci.* **115**, 9503 (2018).
- [51] Y. Qi, P. G. Naumov, M. N. Ali, C. R. Rajamathi, W. Schnelle, O. Barkalov, M. Hanfland, S.-C. Wu, C. Shekhar, Y. Sun, V. Süß, M. Schmidt, U. Schwarz, E. Pippel, P. Werner, R. Hillebrand, T. Förster, E. Kampert, S. Parkin, R. J. Cava *et al.*, Superconductivity in Weyl semimetal candidate  $\text{MoTe}_2$ , *Nat. Commun.* **7**, 11038 (2016).
- [52] Y. Xing, Z. Shao, J. Ge, J. Luo, J. J. Wang, Z. Zhu, J. Liu, Y. Wang, Z. Zhao, J. Yan, D. Mandrus, B. Yan, X.-J. Liu, M. Pan, and J. J. Wang, Surface superconductivity in the type II Weyl semimetal  $\text{TaIrTe}_4$ , *Natl. Sci. Rev.* **7**, 579 (2020).
- [53] S. Cai, E. Emmanouilidou, J. Guo, X. Li, Y. Li, K. Yang, A. Li, Q. Wu, N. Ni, and L. Sun, Observation of superconductivity in the pressurized Weyl-semimetal candidate  $\text{TaIrTe}_4$ , *Phys. Rev. B* **99**, 020503 (2019).
- [54] Q.-G. Mu, F.-R. Fan, H. Borrmann, W. Schnelle, Y. Sun, C. Felser, and S. Medvedev, Pressure-induced superconductivity and modification of fermi surface in type-II Weyl semimetal  $\text{NbIrTe}_4$ , *npj Quantum Mater.* **6**, 55 (2021).
- [55] M. Mandal and R. P. Singh, Emergent superconductivity by re doping in type-II Weyl semimetal  $\text{NiTe}_2$ , *J. Phys.: Condens. Matter* **33**, 135602 (2021).
- [56] G. Shipunov, I. Kovalchuk, B. R. Piening, V. Labracherie, A. Veyrat, D. Wolf, A. Lubk, S. Subakti, R. Giraud, J. Dufouleur, S. Shokri, F. Caglieris, C. Hess, D. V. Efremov, B. Büchner, and S. Aswartham, Polymorphic  $\text{PtBi}_2$ : Growth, structure, and superconducting properties, *Phys. Rev. Mater.* **4**, 124202 (2020).
- [57] S. Schimmel, Y. Fasano, S. Hoffmann, J. Puig, G. Shipunov, D. Baumann, S. Aswartham, B. Buchner, and C. Hess, High-*t* surface superconductivity in topological Weyl semimetal  $t\text{-PtBi}_2$ , *arXiv:2302.08968*.
- [58] F. Fei, X. Bo, P. Wang, J. Ying, J. Li, K. Chen, Q. Dai, B. Chen, Z. Sun, M. Zhang, F. Qu, Y. Zhang, Q. Wang, X. Wang, L. Cao, H. Bu, F. Song, X. Wan, and B. Wang, Band structure perfection and superconductivity in type-II Dirac semimetal  $\text{Ir}_{1-x}\text{Pt}_x\text{Te}_2$ , *Adv. Mater.* **30**, 1801556 (2018).
- [59] H. Wang, H. Wang, H. Liu, H. Lu, W. Yang, S. Jia, X.-J. Liu, X. C. Xie, J. Wei, and J. Wang, Observation of superconductivity induced by a point contact on 3D Dirac semimetal  $\text{Cd}_3\text{As}_2$  crystals, *Nat. Mater.* **15**, 38 (2016).
- [60] L. Aggarwal, A. Gaurav, G. S. Thakur, Z. Haque, A. K. Ganguli, and G. Sheet, Unconventional superconductivity at mesoscopic point contacts on the 3D Dirac semimetal  $\text{Cd}_3\text{As}_2$ , *Nat. Mater.* **15**, 32 (2016).
- [61] L. He, Y. Jia, S. Zhang, X. Hong, C. Jin, and S. Li, Pressure-induced superconductivity in the three-dimensional topological Dirac semimetal  $\text{Cd}_3\text{As}_2$ , *npj Quantum Mater.* **1**, 16014 (2016).
- [62] D. Yan, D. Geng, Q. Gao, Z. Cui, C. Yi, Y. Feng, C. Song, H. Luo, M. Yang, M. Arita, S. Kumar, E. F. Schwier, K. Shimada, L. Zhao, K. Wu, H. Weng, L. Chen, X. J. Zhou, Z. Wang, Y. Shi *et al.*, Superconductivity and Fermi-surface nesting in the candidate Dirac semimetal NBC, *Phys. Rev. B* **102**, 205117 (2020).
- [63] S. Das, Amit, A. Sirohi, L. Yadav, S. Gayen, Y. Singh, and G. Sheet, Conventional superconductivity in the type-II Dirac semimetal  $\text{PdTe}_2$ , *Phys. Rev. B* **97**, 014523 (2018).
- [64] H. Leng, C. Paulsen, Y. K. Huang, and A. de Visser, Type-I superconductivity in the Dirac semimetal  $\text{PdTe}_2$ , *Phys. Rev. B* **96**, 220506 (2017).
- [65] C. Huang, B. T. Zhou, H. Zhang, B. Yang, R. Liu, H. Wang, Y. Wan, K. Huang, Z. Liao, E. Zhang, S. Liu, Q. Deng, Y. Chen, X. Han, J. Zou, X. Lin, Z. Han, Y. Wang, K. T. Law, and F. Xiu, Proximity-induced surface superconductivity in Dirac semimetal  $\text{Cd}_3\text{As}_2$ , *Nat. Commun.* **10**, 2217 (2019).
- [66] H. Leng, A. Ohmura, L. N. Anh, F. Ishikawa, T. Naka, Y. K. Huang, and A. de Visser, Superconductivity under pressure in the Dirac semimetal  $\text{PdTe}_2$ , *J. Phys.: Condens. Matter* **32**, 025603 (2020).
- [67] V. D. Esin, O. O. Shvetsov, A. V. Timonina, N. N. Kolesnikov, and E. V. Deviatov, Interface superconductivity in a Dirac semimetal  $\text{NiTe}_2$ , *Nanomaterials* **12**, 4114 (2022).
- [68] Amit and Y. Singh, Heat capacity evidence for conventional superconductivity in the type-II Dirac semimetal  $\text{PdTe}_2$ , *Phys. Rev. B* **97**, 054515 (2018).
- [69] A. Veyrat, V. Labracherie, D. L. Bashlakov, F. Caglieris, J. I. Facio, G. Shipunov, T. Charvin, R. Acharya, Y. Naidyuk, R. Giraud, J. van den Brink, B. Büchner, C. Hess, S. Aswartham, and J. Dufouleur, Berezinskii-Kosterlitz-Thouless transition in the type-I weyl semimetal  $\text{PtBi}_2$ , *Nano Lett.* **23**, 1229 (2023).
- [70] A. Kuibarov, O. Suvorov, R. Vocaturro, A. Fedorov, R. Lou, L. Merkwitz, V. Voroshnin, J. I. Facio, K. Koepernik, A. Yaresko, G. Shipunov, S. Aswartham, J. van den Brink, B. Büchner, and S. Borisenko, Superconducting arcs, *arXiv:2305.02900*.
- [71] E. Benito-Matías and R. A. Molina, Surface states in topological semimetal slab geometries, *Phys. Rev. B* **99**, 075304 (2019).
- [72] P. Deng, Z. Xu, K. Deng, K. Zhang, Y. Wu, H. Zhang, S. Zhou, and X. Chen, Revealing Fermi arcs and Weyl nodes in  $\text{MoTe}_2$  by quasiparticle interference mapping, *Phys. Rev. B* **95**, 245110 (2017).
- [73] K. Deng, G. Wan, P. Deng, K. Zhang, S. Ding, E. Wang, M. Yan, H. Huang, H. Zhang, Z. Xu, J. Denlinger, A. Fedorov, H. Yang, W. Duan, H. Yao, Y. Wu, S. Fan, H. Zhang, X. Chen, and S. Zhou, Experimental observation of topological Fermi arcs in type-II Weyl semimetal  $\text{MoTe}_2$ , *Nat. Phys.* **12**, 1105 (2016).
- [74] F. Haldane, Attachment of surface “fermi arcs” to the bulk fermi surface: “fermi-level plumbing” in topological metals, *arXiv:1401.0529*.
- [75] P. Hosur, Friedel oscillations due to Fermi arcs in Weyl semimetals, *Phys. Rev. B* **86**, 195102 (2012).
- [76] L. Huang, T. M. McCormick, M. Ochi, Z. Zhao, M. T. Suzuki, R. Arita, Y. Wu, D. Mou, H. Cao, J. Yan, N. Trivedi, and A. Kaminski, Spectroscopic evidence for a type-II Weyl semimetallic state in  $\text{MoTe}_2$ , *Nat. Mater.* **15**, 1155 (2016).
- [77] D. Iaia, G. Chang, T.-R. Chang, J. Hu, Z. Mao, H. Lin, S. Yan, and V. Madhavan, Searching for topological Fermi arcs via quasiparticle interference on a type-II Weyl semimetal  $\text{MoTe}_2$ , *npj Quantum Mater.* **3**, 38 (2018).
- [78] H. Kwon, T. Jeong, S. Appalakondaiah, Y. Oh, I. Jeon, H. Min, S. Park, Y. J. Song, E. Hwang, and S. Hwang, Quasiparticle interference and impurity resonances on  $\text{WTe}_2$ , *Nano Res.* **13**, 2534 (2020).

- [79] A. Lau, K. Koepf, J. Van Den Brink, and C. Ortix, Generic coexistence of Fermi arcs and Dirac cones on the surface of time-reversal invariant Weyl semimetals, *Phys. Rev. Lett.* **119**, 076801 (2017).
- [80] M. Sakano, M. S. Bahramy, H. Tsuji, I. Araya, K. Ikeura, H. Sakai, S. Ishiwata, K. Yaji, K. Kuroda, A. Harasawa, S. Shin, and K. Ishizaka, Observation of spin-polarized bands and domain-dependent Fermi arcs in polar Weyl semimetal MoTe<sub>2</sub>, *Phys. Rev. B* **95**, 121101 (2017).
- [81] S. Y. Xu, I. Belopolski, D. S. Sanchez, C. Zhang, G. Chang, C. Guo, G. Bian, Z. Yuan, H. Lu, T. R. Chang, P. P. Shibayev, M. L. Prokopovych, N. Alidoust, H. Zheng, C. C. Lee, S. M. Huang, R. Sankar, F. Chou, C. H. Hsu, H. T. Jeng *et al.*, Experimental discovery of a topological Weyl semimetal state in TaP, *Sci. Adv.* **1**, (2015).
- [82] S. Y. Xu, C. Liu, S. K. Kushwaha, R. Sankar, J. W. Krizan, I. Belopolski, M. Neupane, G. Bian, N. Alidoust, T. R. Chang, H. T. Jeng, C. Y. Huang, W. F. Tsai, H. Lin, P. P. Shibayev, F. C. Chou, R. J. Cava, and M. Z. Hasan, Observation of Fermi arc surface states in a topological metal, *Science* **347**, 294 (2015).
- [83] Q. Xu, E. Liu, W. Shi, L. Muechler, J. Gayles, C. Felser, and Y. Sun, Topological surface Fermi arcs in the magnetic Weyl semimetal Co<sub>3</sub>Sn<sub>2</sub>S<sub>2</sub>, *Phys. Rev. B* **97**, 235416 (2018).
- [84] Y. Yuan, X. Yang, L. Peng, Z.-J. Wang, J. Li, C.-J. Yi, J.-J. Xian, Y.-G. Shi, and Y.-S. Fu, Quasiparticle interference of Fermi arc states in the type-II Weyl semimetal candidate WTe<sub>2</sub>, *Phys. Rev. B* **97**, 165435 (2018).
- [85] Q.-Q. Yuan, L. Zhou, Z.-C. Rao, S. Tian, W.-M. Zhao, C.-L. Xue, Y. Liu, T. Zhang, C.-Y. Tang, Z.-Q. Shi, Z.-Y. Jia, H. Weng, H. Ding, Y.-J. Sun, H. Lei, and S.-C. Li, Quasiparticle interference evidence of the topological Fermi arc states in chiral fermionic semimetal CoSi, *Sci. Adv.* **5**, (2019).
- [86] C. Zhang, A. Narayan, S. Lu, J. Zhang, H. Zhang, Z. Ni, X. Yuan, Y. Liu, J.-H. Park, E. Zhang, W. Wang, S. Liu, L. Cheng, L. Pi, Z. Sheng, S. Sanvito, and F. Xiu, Evolution of Weyl orbit and quantum Hall effect in Dirac semimetal Cd<sub>3</sub>As<sub>2</sub>, *Nat. Commun.* **8**, 1272 (2017).
- [87] P. J. W. Moll, N. L. Nair, T. Helm, A. C. Potter, I. Kimchi, A. Vishwanath, and J. G. Analytis, Transport evidence for Fermi-arc-mediated chirality transfer in the Dirac semimetal Cd<sub>3</sub>As<sub>2</sub>, *Nature (London)* **535**, 266 (2016).
- [88] A. C. Potter, I. Kimchi, and A. Vishwanath, Quantum oscillations from surface Fermi arcs in Weyl and Dirac semimetals, *Nat. Commun.* **5**, 5161 (2014).
- [89] Y. Zhang, D. Bulmash, P. Hosur, A. Potter, and A. Vishwanath, Quantum oscillations from generic surface Fermi arcs and bulk chiral modes in Weyl semimetals, *Sci. Rep.* **6**, (2016).
- [90] J. Bardeen, L. N. Cooper, and J. R. Schrieffer, Theory of Superconductivity, *Phys. Rev.* **108**, 1175 (1957).
- [91] H. K. Pal, O. E. Obakpolor, and P. Hosur, Anomalous surface conductivity of Weyl semimetals, *Phys. Rev. B* **106**, 245410 (2022).
- [92] O. E. Obakpolor and P. Hosur, Surface Luttinger arcs in Weyl semimetals, *Phys. Rev. B* **106**, L081112 (2022).